The magnetospheric banana current

Michael W. Liemohn,[1] Natalia Yu. Ganushkina,[1] Roxanne M. Katus,[1]
Darren L. De Zeeuw,[1] and Daniel T. Welling[1]

Received 5 October 2012; revised 23 January 2013; accepted 25 January 2013; published 1 March 2013.

[1] It is shown that the banana current, a current system in the inner magnetosphere closing entirely within the magnetosphere (i.e., not through the ionosphere or on the magnetopause) but not circumflowing around the Earth, is a regular feature of near-Earth space. Closure options for the eastward asymmetric current on the inside of a localized pressure peak were explored, with the conclusion that the current must close via westward current around the outside of the high pressure region. It is a current that encircles a pressure peak and, therefore, whenever there is a pressure peak in the inner magnetosphere, a banana current exists. If multiple pressure peaks exist in the inner magnetosphere, then multiple banana currents will also coexist. Its occurrence rate is equal to that of the partial ring current, defined here as westward magnetospheric current that closes through field-aligned currents into and out of the ionosphere. Its magnitude can reach a few mega-amps during the main phase of storms, but drops to <0.1 MA during extended quiet intervals. The magnetic perturbation related to this current is strong within the region of high plasma pressure that it encircles, but is otherwise very weak outside of the banana current loop because the oppositely-directed current flow on either side of the loop largely cancels each other. In general, its related magnetic field is a few nanotesla of northward perturbation for both ground-based and geosynchronous magnetometers, making it difficult to magnetically detect. The banana current is placed in the context of the other near-Earth nightside current systems.

Citation: Liemohn, M. W., N. Y. Ganushkina, R. M. Katus, D. L. De Zeeuw, and D. T. Welling (2013), The magnetospheric banana current, *J. Geophys. Res. Space Physics*, *118*, 1009–1021, doi:10.1002/jgra.50153.

1. Introduction

[2] There are several current systems that flow in the near-Earth nightside magnetosphere. In particular, three systems are commonly mentioned: the symmetric ring current, the partial ring current, and the magnetotail current. Since the discovery of asymmetries in the inner magnetospheric plasma pressure [*Frank*, 1970], the definition, identification, evolution, and relative importance of these currents are long-discussed yet still-open topics of research in magnetospheric physics [e.g., *Mauk and Zanetti*, 1987; *Iyemori*, 1990; *Lui and Hamilton*, 1992; *Alexeev et al*., 1996; *Antonova and Ganushkina*, 1997; *Siscoe et al*., 2000; *Antonova and Ganushkina*, 2000; *Turner et al*., 2000; *Ohtani et al*., 2001, 2007; *Liemohn et al*., 2001, 2011; *Ganushkina et al*., 2002, 2004, 2010, 2012; *Kalegaev et al*., 2005; *Tsyganenko et al*., 2003; *Daglis et al*., 2003; *Antonova*, 2004; *Daglis*, 2006; *Pulkkinen et al*., 2006; *Kubyshkina et al*., 2008]. Understanding these issues regarding the partitioning of inner magnetospheric currents is important because each one contributes uniquely to the distortion of the electric and magnetic fields of the region. However, before these questions can be addressed, it is useful to define to what each of these three terms is referring.

[3] The symmetric ring current is often defined as the part of the cross-magnetic-field current density ($\mathbf{J}_\perp$) which circumflows the Earth, closing on itself. This is created by the inner magnetospheric pressure peak that circumscribes the Earth, formed by hot ions trapped on closed drift paths, gradient-curvature drifting around the Earth. Typically, there is a larger westward component outside of the pressure peak and a smaller amplitude eastward current Earthward of the peak (see, for example, the AMPTE/CCE data analyzed by *Lui et al*. [1987]).

[4] The near-Earth partial ring current can be defined as the part of the westward $\mathbf{J}_\perp$ in the magnetosphere that closes through field-aligned currents ($\mathbf{J}_\parallel$) into and out of the ionosphere. Specifically, the configuration is usually oriented with the magnetospheric $\mathbf{J}_\perp$ starting in the post-midnight sector and extending into the pre-midnight sector with $\mathbf{J}_\parallel$ out of the ionosphere at the eastward end and into the ionosphere at the westward end. Ionospheric currents complete the loop based on the spatial distribution of conductance.

[5] Near-Earth magnetotail currents are typically defined as the part of $\mathbf{J}_\perp$ that closes on the magnetopause. Specifically, this current flows from the dawnside to the duskside across the plasma sheet and then bifurcates to close via a magnetopause current around the magnetotail lobes back to the dawnside.

[1]Atmospheric, Oceanic, and Space Sciences Department, University of Michigan, Ann Arbor, Michigan, USA.

Corresponding author: M. W. Liemohn, Atmospheric, Oceanic, and Space Sciences Department, University of Michigan, 2455 Hayward St., Ann Arbor, MI 48109-2143, USA. (liemohn@umich.edu)

2169-9380/13/10.1002/jgra.50153

[6] There is one more current system in the inner magnetosphere that does not fit within these definitions. This undefined current is most readily seen in the local time asymmetry of the eastward $\mathbf{J}_\perp$ deep within near-Earth space. A local time asymmetry of the plasma pressure distribution, as seen in charged particle data [e.g., *Frank*, 1970; *Lui et al*., 1994; *Milillo et al*., 2001; *Jorgensen et al*., 2004; *Runov et al*., 2008; *Ganushkina et al*., 2012] and energetic neutral atom images [e.g., *Roelof*, 1987; *Henderson et al*., 1997; *Mitchell et al*., 2001; *Pollock et al*., 2001; *Perez et al*., 2001; *Brandt et al*., 2002a, 2002b; *Roelof et al*., 2004; *Valek et al*., 2010; *Buzulukova et al*., 2010] will yield an asymmetry in both the westward and eastward currents around it [e.g., *Vasyliunas*, 1970; *Antonova and Ganushkina*, 1997; *Tsyganenko et al*., 2003]. Several questions remain unresolved about the asymmetric eastward current. First, how does this current segment close? One possibility is that it closes as a reverse partial ring current through region-3 type $\mathbf{J}_\parallel$. Another possibility is that it is closed within the magnetosphere by westward $\mathbf{J}_\perp$. Second, how often does it exist? It could be a storm-time phenomenon or a ubiquitous feature of the inner magnetosphere. Third, what are its typical and extreme intensities? They could be either an insignificant factor to the overall magnetospheric topology or a necessary and integral component of the magnetic field configuration of near-Earth space. Fourth and final, what is the expected magnetic perturbation associated with this current system? It could be either a minor factor in the overall magnetic distortion of geospace or a dominant contributor to internally produced topological changes. These questions are explored below.

2. Closure Analysis

[7] When there is a local time asymmetry in the eastward $\mathbf{J}_\perp$ deep within the inner magnetosphere, it must close somehow through another part the geospace system. There are two obvious possibilities for this closure path: through field-aligned currents and the ionosphere and through a westward $\mathbf{J}_\perp$ just beyond the eastward current. First, consider the equation governing the formation of perpendicular current. It can be presented a function of pressure anisotropy and perpendicular pressure gradient [e.g., *Parker*, 2000]:

$$J_\perp = \frac{\mathrm{B}}{B^2} \times \left[\nabla P_\perp + \left(P_\parallel - P_\perp\right) \frac{\nabla B}{B} \right] \tag{1}$$

where an eastward current is defined as a positive $\mathbf{J}_\perp$. Because $\mathbf{B}$ is northward and ∇B is Earthward in the inner magnetosphere, an eastward current is generated when the pressure gradient is outward (i.e., the chosen location is Earthward of the pressure peak) or when $P_\perp$ is greater than $P_\parallel$. *Lui et al*. [1987] and *Lui* [2003] analyzed inner magnetospheric plasma pressure data and concluded that it is often either nearly isotropic or anisotropic in a pancake formation, with $P_\perp > P_\parallel$. Furthermore, they concluded that the pressure gradient term is often dominant over the pressure anisotropy term. A pressure anisotropy large enough to dominate equation (1) requires a large drop in $P_\parallel$ relative to $P_\perp$, which might be possible given enough time for charge exchange to deplete those ions mirroring at lower altitudes along the field lines. This, however, would lead to a drop in total pressure and, after Coulomb or wave-particle scattering, most likely a drop in $P_\perp$ closer to Earth, which would create an eastward current due to the first term in equation (1).

[8] Figure 1 shows a schematic of the two possibilities for current closure of an asymmetric eastward $\mathbf{J}_\perp$ (the red arrows). In this diagram, it is assumed that the excess current is formed from a localized pressure peak within the inner magnetosphere. The two current closure options are designated as "path 1" (the $\mathbf{J}_\parallel$ route, in orange) and "path 2" (the westward $\mathbf{J}_\perp$ route, in purple). Also shown in Figure 1 are the isocontours and gradients of plasma pressure (in blue) and flux tube volume (in green).

[9] To consider the "path 1" option of $\mathbf{J}_\parallel$ closure, it is useful to examine the equations that lead to the formation of field-aligned currents. The Vasyliunas equation defines $\mathbf{J}_\parallel$ as a function of the plasma pressure gradient in and the flux tube volume gradient [*Vasyliunas*, 1970]:

$$J_{\parallel,i} = \frac{Bi}{2B_{eq}^2} \left(\nabla P_{eq} \times B_{eq}\right).\nabla_{eq} \left(\int \frac{dl}{B} \right) \tag{2}$$

where the subscripts "i" and "eq" denote quantities taken at the ionospheric footpoint and equatorial plane crossing of the field line under consideration, and the integral is along this same magnetic field line. The resulting current is defined as positive when flowing into the ionosphere and negative when flowing out of it. Note that *Birmingham* [1992] extended this formula to give the field-aligned current that accumulates between any two points along a magnetic field line including the effects of an anisotropic pressure distribution. For the present study, the Vasyliunas equation is adequate.

[10] The schematic in Figure 1 shows the relationship of gradients in the equatorial plane with respect to each other. The flux tube volume isocontours point outward with a bit of deviation away from the pressure peak (due to the diamagnetic effect). The plasma pressure gradients point towards the center of the pressure peak. Field-aligned currents

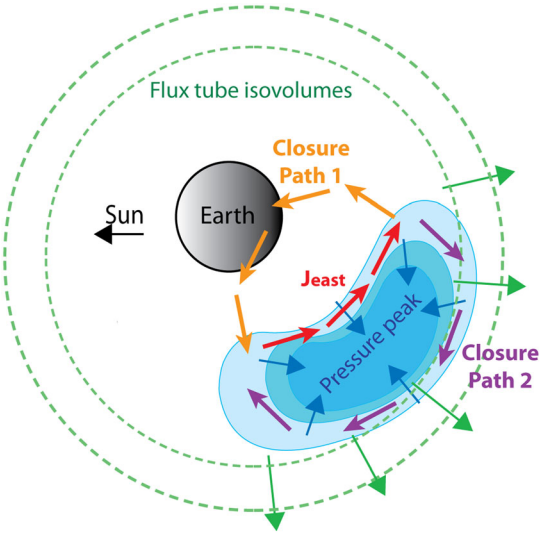

Figure 1. A schematic of the eastward near-Earth current (red arrows) relative to plasma pressure (blue shading) and magnetic flux tube volume isocontours (green dashed lines). Plasma pressure gradients (blue arrows) and flux tube isocontour gradients (green arrows) are also shown. The two options for closure of the eastward current are shown (path 1 in orange and path 2 in purple).

are generated where these two gradient vectors are perpendicular, i.e., when the pressure gradient is nearly azimuthal at the eastern and western ends of the pressure peak. Therefore, equation (2) yields a field-aligned current out of the ionosphere on the eastern end of the pressure peak and a current into the ionosphere on the western end of the peak. These are region 2 field-aligned currents closing the partial ring current and setting up the electric field shielding effect in the inner magnetosphere. In order to obtain a "region 3-type" field-aligned current equatorward of these currents, the pressure gradient would have to reverse inside of the main pressure peak. This implies the existence of a very strange pressure peak configuration in the inner magnetosphere, with additional peaks Earthward and offset in local time from the main peak. While this could happen (given subsequent injections from the plasma sheet into the inner magnetosphere), these additional peaks would have their own region 2-type field-aligned currents associated with them. The excess eastward $\mathbf{J}_\perp$ near the pressure peak should close on a path independent of other injections and peaks and, therefore, closure path 1 is unfeasible.

[11] Closure path 2, however, fits naturally with the pressure gradients shown in Figure 1 and the $\mathbf{J}_\perp$ formula in equation (1). Let us take a closer examination of this option. This outer, westward $\mathbf{J}_\perp$ is also associated with the partial ring current, which closes through $\mathbf{J}_\parallel$ at each end of the pressure peak. As long as the westward $\mathbf{J}_\perp$ is large enough to supply both the $\mathbf{J}_\parallel$ and the eastward inner $\mathbf{J}_\perp$, then this is the correct closure path. To assess the possibility of both of these currents flowing on the outer portion of a pressure peak, let us consider a simplified scenario: radial pressure profile with a peak at L_{Pmax} that decreases to zero at a distance ΔL_{P} away (with some functional form), a dipolar magnetic field normalized to unity at the pressure peak, and an isotropic pressure distribution. A schematic of this idealized case is shown in Figure 2. Figure 2a shows two pressure profile cases, one with a linear slope and another with a downward parabolic shape. Figure 2b shows two magnetic field variations across this radial extent, one steeper than the other, representing a "thin" and a "wide" pressure peak (the wide option is steeper than the thin one). Both of these are normalized to the magnetic field strength at L_{Pmax}. Figure 2c shows the resulting $\mathbf{J}_\perp$ from these pressure and magnetic field distributions. All three curves clearly show that the outer westward current density is larger than the inner eastward current density, with the disparity increasing as the extrema of the pressure gradients are moved farther apart. To compare total current, this current density must be integrated over the cross-sectional area of the current, which is not only the width ΔL_{P} but also the length along the field line (which is a function of L, and increases for larger L). This yields a total eastward current that is only 7% to 21% of the total westward current for these three scenarios.

[12] From these idealized examples, it can be inferred that there is ample current on the outside of the pressure peak not only to supply the partial ring current but also to close the eastward current on the inside of the pressure peak. In fact, for these cases, the partial ring current is 3.8 to 13.3 times larger than the current loop encircling the pressure peak. Thus, closure path 2 is the most likely option. The morphology of this current system is, therefore, a thin crescent shape similar to the pressure peak in the inner magnetosphere. Because of this characteristic shape, hereinafter, we shall call this current system the "banana current".

3. Occurrence and Magnitude Analysis

[13] The next questions to address are how often the banana current exists within the inner magnetosphere and what is its typical intensity. As seen in the section above, it encircles a pressure peak; therefore, an initial hypothesis about its occurrence is that it is formed after every injection from the plasma sheet and lasts for several hours, i.e., until the energy-dependent drifts of the particles spread out the localized pressure peak into a symmetric shell around the Earth. Furthermore, the relative magnitude from the idealized pressure peaks in the section above yielded a total intensity for the banana current several times smaller than the partial ring current generated by that peak. The magnitude of the banana

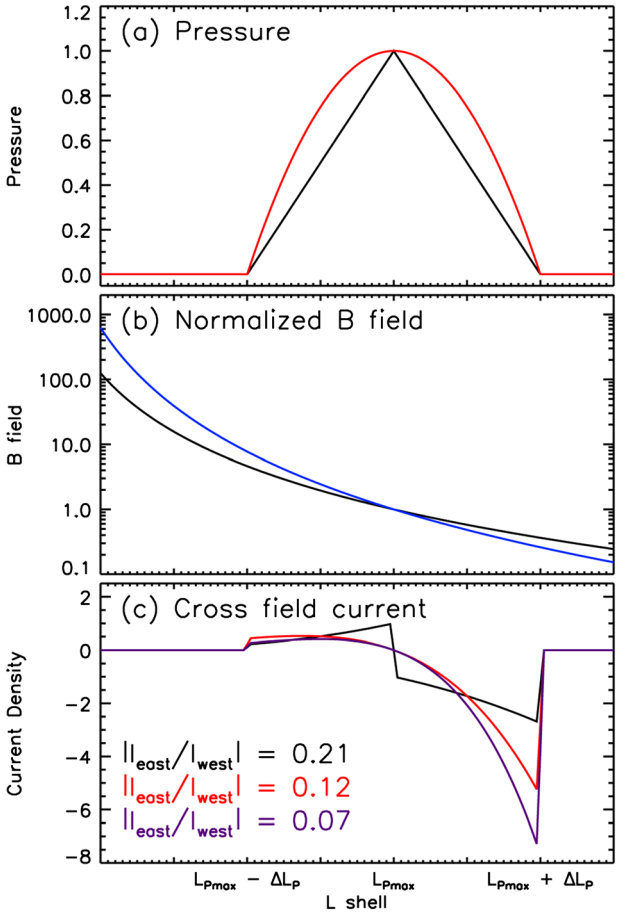

Figure 2. Idealized pressure and magnetic field profiles and the resulting current density. (a) The black line has a linear slope while the red line is a parabola. (b) The black and blue lines represent a "thin" and "wide" ΔL extent of the pressure peak, respectively. Both have been normalized to the value as L_{Pmax}. (c) The black line current density is based on the linear pressure and "thin" B profile, the red line is based on the parabolic pressure and "thin" B profile, and the purple line is based on the parabolic pressure and "thick" B profile. The total current values used in the ratios assumed an isotropic pressure along the field line.

current can be analyzed more rigorously and placed into the context of other current systems, by considering numerical simulation results. First, however, let us discuss how we will define and calculate current systems from numerical simulation results.

3.1. Current System Calculation Methodology

[14] There are two contributors to the eastward current: the eastward symmetric ring current and the banana current. The eastward symmetric ring current is the easier of the two to define, as it is simply the minimum azimuthal current in the eastward direction. This is the amount of eastward current circumflowing around the Earth. The banana current is a bit more problematic to define because of the possible existence of multiple peaks. The easiest definition would be the maximum eastward current minus the minimum eastward current, but this would underestimate the banana current whenever there is more than one pressure peak in the simulation domain. Therefore, another method was devised: adding the eastward current for each relative maxima separately. In particular, only the differential part of the current from the nearest minima should be added in; otherwise, a double counting (and therefore overestimate) would result. The formula can be expressed as follows: scanning in magnetic local time (MLT), if the eastward current at MLT location j is larger than the eastward current at MLT location $j - 1$, then the difference between these two currents is added to the banana current total for that time. If only one pressure peak exists, then this formula is equivalent to the maximum minus minimum difference. If multiple peaks exist at a given time, then this method adds the contributions from each eastward current peak, but only the amount above the nearest relative minimum in the eastward current. While this is not a perfect calculation of the banana current and still could underestimate the intensity of all of the banana currents at any one time (if the current systems overlap in MLT in a way that obscures their true magnitudes, or if part of the banana current is beyond the simulation domain), it should yield a value very close to the true total.

[15] To obtain the other current system magnitudes, some other current quantities need to be extracted from a numerical simulation. The inward (outward) field-aligned currents are summed to yield totals in each direction as a function of local time. The inward and outward field-aligned currents are then separately summed to yield a total field-aligned current value for each time. The radial current through the outer boundary is also summed along the field line to provide the current flowing into and out of the simulation domain. For an inner magnetospheric drift physics model, this outer boundary is at the outermost grid cell face. Again, the inward and outward radial currents are summed separately to yield a total current flowing through the outer boundary of the simulation domain.

[16] The magnitudes of the other near-Earth current systems (as a function of time) are then defined from these quantities. The eastward (westward) symmetric ring current is defined as the minimum azimuthal current in the eastward (westward) direction. The partial ring current is defined as the total current flowing into or out of the ionosphere, whichever value is larger. The larger of the two field-aligned current totals is used because some of the partial ring current could be beyond the simulation domain; therefore, anything flowing either into or out of the ionosphere within the simulation domain is partial ring current. The tail current is defined as the total current flowing into or out of the simulation domain through the outer boundary, whichever value is smaller. The smaller of the two radial current totals is used because some of the radial outer boundary current could belong to a different current system. The tail current is defined as the current that closes on the magnetopause; therefore, if it enters the simulation domain (through the outer boundary), it must also leave it the same way.

3.2. Application to a Magnetic Storm

[17] Let us consider the current systems from the drift physics modeling conducted by *Liemohn et al*. [2006]. That study used the Hot Electron and Ion Drift Integrator (HEIDI) model, which solves the gyration- and bounce-averaged kinetic equations for the phase space density of hot (~keV) plasma species in the inner magnetosphere (specifically, inside of the geosynchronous orbit, with an outer boundary at 6.625 R_E) [*Fok et al*., 1993; *Jordanova et al*., 1994; *Liemohn et al*., 1999]. One of the events considered by that study was the 21–23 October 2001 magnetic storm, which reached –187 nT at 2100 UT on 21 October with a second *Dst* minimum of −165 nT at 0000 UT on 23 October. The main phase was only 5 h long, which is relatively fast compared to most intense magnetic storms [cf., *Pulkkinen et al*., 2007; *Ilie et al*., 2008; *Katus et al*., 2012]. It is chosen here because the prestorm magnetosphere is very quiet and the peak storm intensity is large, implying a rapid development and evolution of the inner magnetospheric current systems. With its multiple *Dst* minima, it contains several injection sequences from the tail, including a sawtooth interval early on 22 October [see, e.g., *Pulkkinen et al*., 2006].

[18] *Liemohn et al*. [2006] conducted several simulations for this storm, using various electric fields and comparing against a large assortment of space- and ground-based data sets. Two of these simulations will be considered here: that with a Volland-Stern (V-S) electric field description driven by the 3-h cadence *Kp* index [*Volland*, 1973; *Stern*, 1975; *Maynard and Chen*, 1975] and the self-consistent (S-C) electric field approach of *Liemohn et al*. [2004, 2005], which uses the currents within HEIDI to modify the midlatitude ionospheric potential pattern each time step. These two options were the best at matching the various data sets included in the comparison.

[19] From these simulation results, the cross-field currents are computed using equation (1), and field-aligned currents are calculated as a divergence of the total cross-field current, integrated along each field line, as was done by *Liemohn et al*. [2001]. Figure 3 shows the equatorial plane azimuthal current density at six times during the October 2001 magnetic storm interval, from before the storm sudden commencement (Figure 3a) through the main phase (Figures 3b–3e) to the storm peak (Figure 3f) and one in the late recovery phase after the secondary storm peak (Figure 3g). The Sun is to the left in this bird's-eye view over the North Pole, with the red/yellow colors being eastward current and the blue/green colors showing westward current.

[20] The Volland-Stern electric field is defined by an analytical formula and, in the version used here, is driven by the 3-h *Kp* index. This field produces a smooth electric potential pattern and subsequently a smooth, crescent-shaped pressure

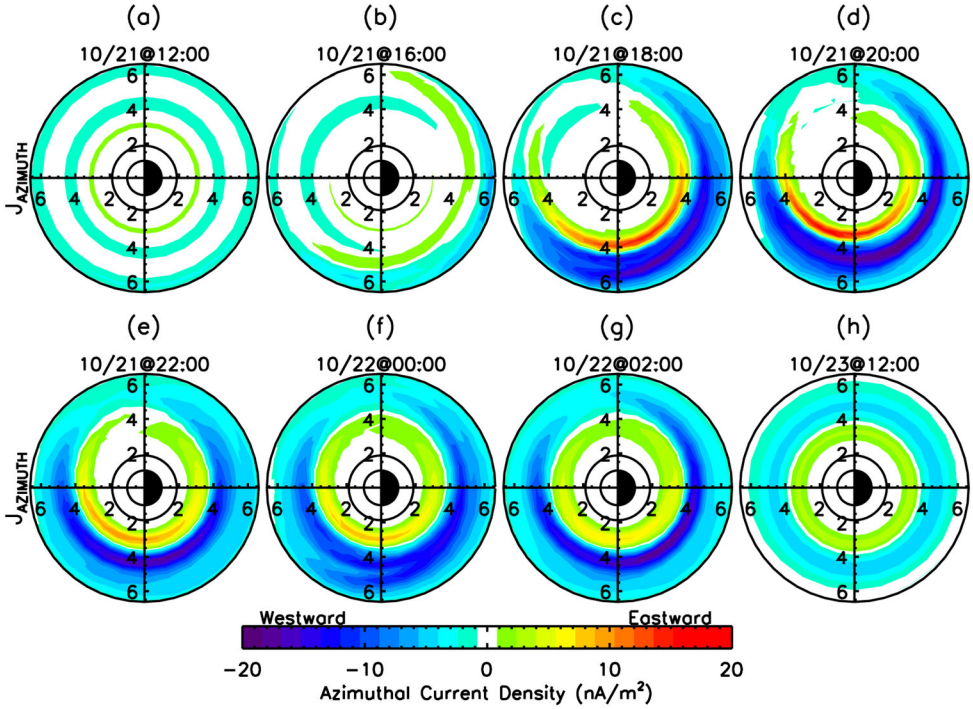

Figure 3. Azimuthal current densities in the equatorial plane during the 21–23 October 2001 magnetic storm as calculated from the HEIDI simulation with the V-S electric field description. The view is from over the North Pole with the Sun to the left; distances are given in Earth radii with results shown from $L = 2$ to 6.5.

peak, often (but not always) just a single peak. It is, therefore, the easier of the two simulation results to examine. It is seen in Figure 3 that the azimuthal current density resulting from this electric field is indeed rather smoothly varying. Multiple peaks can form (see Figure 3f) when there are two partial ring currents flowing around separate pressure peaks, but most of the plots contain only a single local time asymmetry peak in the eastward and westward currents.

[21] In the self-consistent electric field description, the plasma pressure calculated by HEIDI is used to calculate $\mathbf{J}_\perp$ and $\mathbf{J}_\parallel$ in the simulation domain, which in turn alters the electric potential pattern. Specifically, this feedback sets up electric potential well-peak pairs at the eastern and western ends of each pressure peak [e.g., *Jaggi and Wolf*, 1973; *Fok et al.*, 2001; *Ridley and Liemohn*, 2002], which results in vortical flows that tend to break up the initial pressure peak into several smaller peaks [e.g., *Liemohn and Brandt*, 2005] and to shift the pressure peak eastward as new injections are diverted in that direction [e.g., *Brandt et al.*, 2002a; *Fok et al.*, 2003; *Ilie et al.*, 2008]. This leads to a different plasma pressure morphological evolution throughout the storm sequence, hindering the ability of subsequent injections to add to an existing partial ring current as well as delaying and suppressing the formation of a symmetric ring current.

[22] Figure 4 presents seven equatorial plane azimuthal current density plots from the S-C electric field HEIDI simulation for this event. The systematic differences with the V-S electric field results, mentioned above, are evident when comparing Figures 3 and 4. The current density is similar in its overall locations for the eastward and westward currents, but the S-C electric field has many small-scale relative maxima within each current region.

[23] At each MLT coordinate, the field lines with eastward (westward) azimuthal current are separately summed, both along the field line and in radial distance, to give total currents in each direction as a function of local time around the Earth. Figure 5 shows these directional azimuthal current values as a function of magnetic local time for one of the plots in Figures 3 and 4, specifically, 1800 UT, during the main phase of the storm. It is seen that, at all local times for both the simulation results, the westward current is larger than the eastward current. With the V-S electric field, the azimuthal currents are rather smooth and nearly sinusoidal, with a peak current around 18–20 MLT and a minimum somewhere in the morning sector. This is a typical main phase current distribution from the V-S electric field. For the S-C electric field simulation, the currents have the same basic structure of a prenoon minimum and premidnight maximum, but with many relative extrema due to the small-scale structure of the pressure distribution.

[24] Figure 6 shows the current analysis results for the October 2001 storm interval from the Volland-Stern electric field HEIDI simulation. Current system magnitudes, as calculated by the methodology presented above, are shown in Figure 6a for the eastward currents and in Figure 6c for the westward currents. These magnitudes are converted into percentages of the total current in each direction and shown in Figures 6b and 6d for the eastward and westward current systems, respectively. For reference, the observed and modeled *Dst** time series are shown in Figure 6f.

[25] Figure 6a presents the magnitudes of the eastward current systems, namely the banana current and the eastward symmetric ring current. It is seen that the banana current quickly builds during the main phase, from a prestorm level

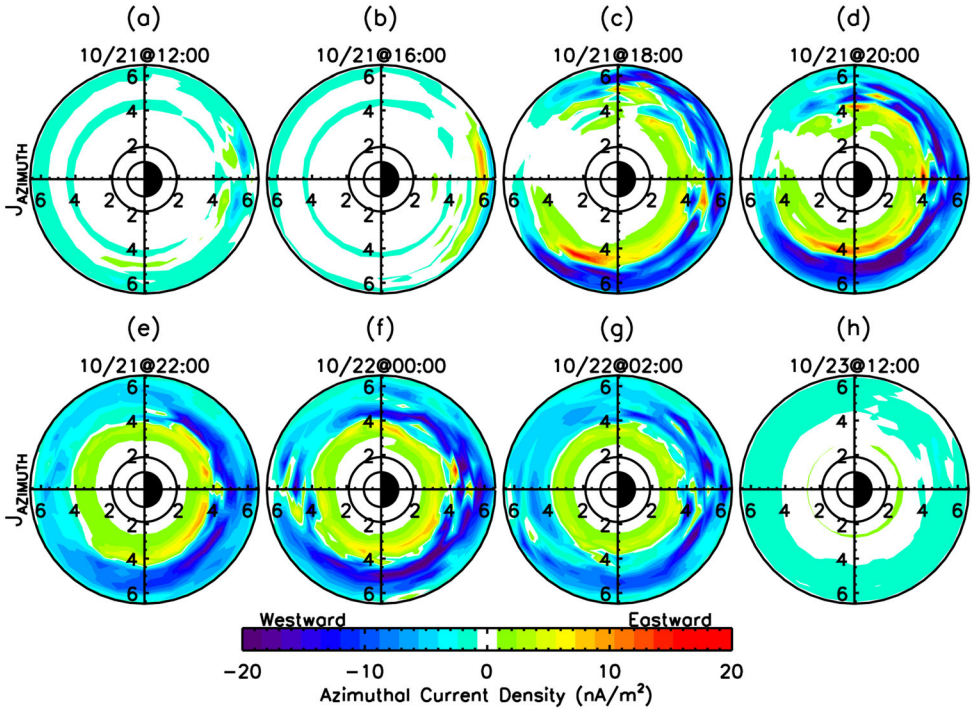

Figure 4. Like Figure 3 except for the HEIDI simulation with the S-C electric field description.

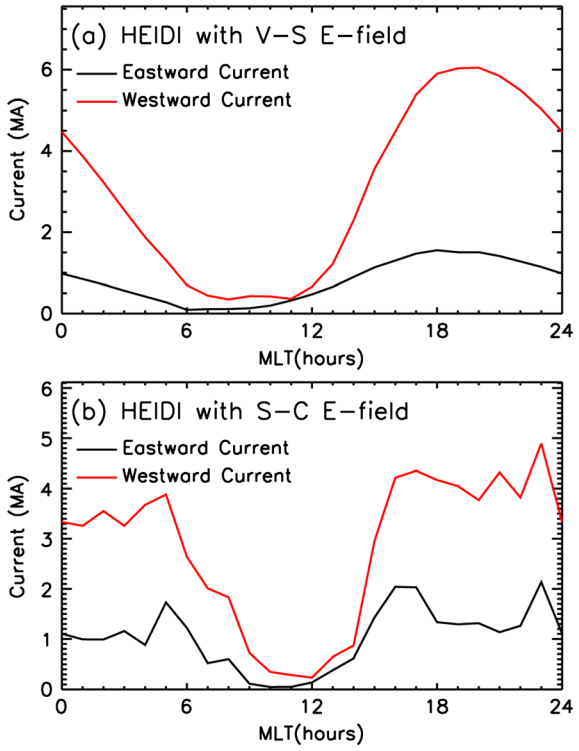

Figure 5. Azimuthal eastward (black lines) and westward (red lines) currents as a function of magnetic local time (integrated over radial distance and magnetic latitude where the azimuthal current density was positive and negative, respectively) at 1800 UT on 21 October 2001, during the main phase of the storm. Shown are results from HEIDI with the (a) V-S electric field and (b) S-C electric field.

of <0.1 MA up to 1.6 MA. Its intensity peaks in the late main phase and drops back to prestorm levels within 4 h of the modeled storm peak. Later injections from the plasma sheet re-intensify the banana current, peaking at 0.9 MA just before the second storm peak. In the late recovery phase, the banana current intensity sinks to ~0.01 MA. The eastward symmetric ring current, however, has a different timing through the storm. It starts to rise from its prestorm value of ~0.1 MA during the latter half of the main phase, reaching a peak value of 0.5 MA in the early recovery phase. It decreases a bit during the later injections and then rises to a second peak value of 0.3 MA early on 23 October. The recovery of this current system is very slow; it still has a value of 2.1 MA at the end of that day.

[26] Figure 6b shows these same current systems as a percentage of the sum of these two eastward currents (i.e., these two curves add up to 100% at each time step). There are several intervals during this storm where the eastward current is almost entirely asymmetric. The reverse is true during the recovery periods, especially the late recovery phase near the end of the interval. The duration of banana current dominance over the eastward symmetric ring current varies from 2 to 11 h during this event for this HEIDI setup configuration.

[27] The magnitudes of the westward current systems are presented in Figure 6c. In addition to the banana current (same values as in Figure 6a), there are also the westward symmetric ring current, the partial ring current, and the tail current. It is seen that the banana current is small compared to the partial ring current and westward symmetric ring current. The timings of the banana current intensifications closely mimic those of the partial ring current. The partial ring current, however, is several times larger than the banana current, with prestorm/poststorm levels of ~0.01 MA and peak values of 4.8 and 3.5 MA just before the two *Dst** minima, respectively. The westward symmetric ring current has

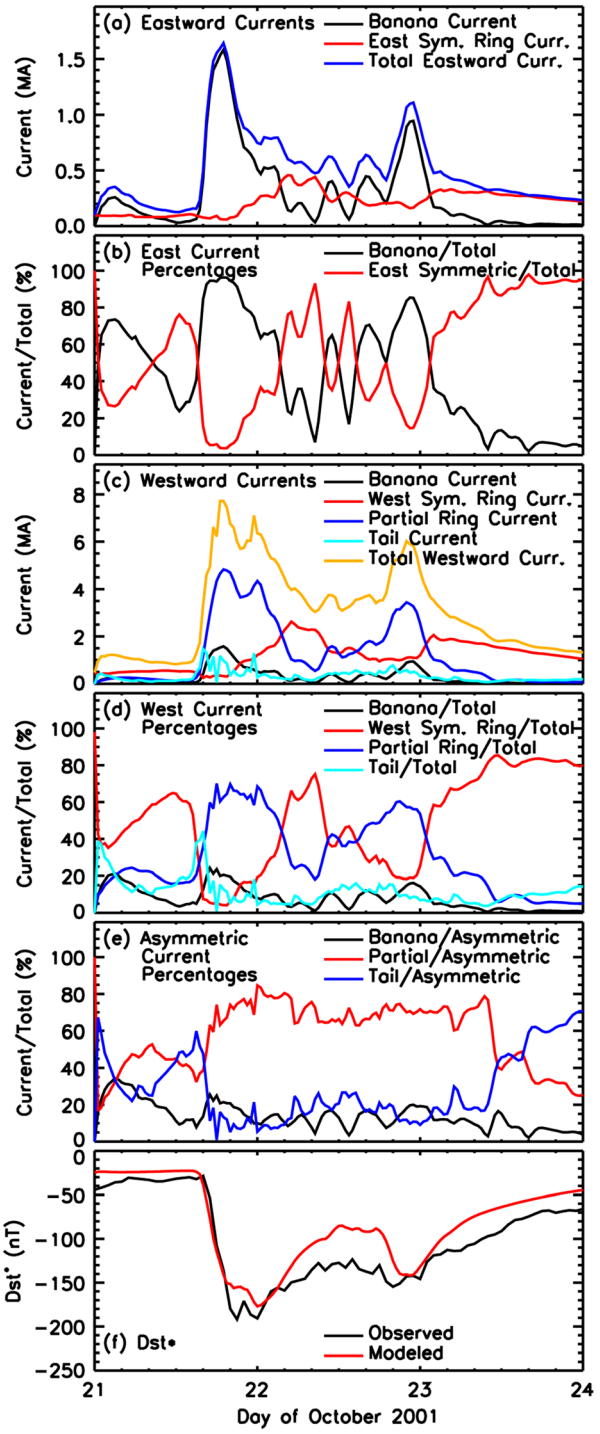

Figure 6. Analysis of currents from a HEIDI simulation with a V-S electric field of the 21 October 2001 magnetic storm (3-day timeline along the x axis). Shown are (a) eastward current intensities, (b) eastward currents as a percentage of the total eastward current, (c) westward current intensities, (d) westward currents as a percentage of the total westward current, (e) westward current percentages without the symmetric ring current included (i.e., only asymmetric currents in the total), and (f) observed and modeled *Dst** time series.

similar intensification timings as the eastward symmetric ring current in Figure 6a. Its prestorm value is ~0.5 MA, initially decreasing during the main phase (as the pre-existing ring current is evacuated from the inner magnetosphere) and subsequently peaking during the two recovery intervals at 2.8 and 2.2 MA, respectively. It recovers faster than the eastward symmetric ring current, dropping to 1 MA by the end of 23 October. The tail current (as simulated by HEIDI within geosynchronous orbit) has a timing and magnitude similar to those of the banana current, although peaking an hour or two earlier. It has a peak intensity of 1.5 MA just prior to the banana current peak during the first main phase on 21 October.

[28] Figure 6d shows the percentages of these current systems relative to the total westward current (again, these curves add up to 100% for any given time). The pre- and poststorm quiet times are dominated by the westward symmetric ring current, while the main and early recovery phases are partial ring current-dominated. There is a brief interval (roughly an hour long) at the start of the first main phase where the tail current is the dominant westward current in the HEIDI simulation. At other times, however, it hovers around the 10% level. The banana current rises to values near 20% during the main phase portions of the event, but then drops below 5% during extended quiet times.

[29] Of the four westward current systems under investigation, three of them are "asymmetric" in that they do not flow completely around the Earth. It is interesting to compare these three currents against one another to understand the relative role each plays in defining the current asymmetry. Figure 6e, therefore, shows the percentages of these three current systems with respect to their summed magnitudes (i.e., like Figure 6d, but excluding the westward symmetric ring current from the total). It is seen that at no point does the banana current dominate, but rather it is a consistent contributor at the 10% to 20% level to the current asymmetry. The majority of the asymmetric current is provided by the tail current initially, at the beginning of an injection sequence, followed by the partial ring current throughout most of the main and early recovery phases. During the late recovery phase, all of these current systems have very small magnitudes (<0.2 MA), but the tail current is systematically larger than the other two and dominates any asymmetry that does exist.

[30] Figure 7 shows a similar sequence of current system results as in Figure 6, except for the HEIDI simulation with the self-consistent electric field description. Again, Figures 7a–7e show the magnitudes and percentages of the eastward and westward current systems, and the *Dst** data-model comparison is shown in Figure 7f for reference.

[31] Figure 7a shows the magnitudes of the eastward currents for this second simulation of the October 2001 storm. Note that the total eastward current line (blue curve) is often on top of the banana current line (black curve) because the eastward symmetric ring current is comparatively small. The banana current intensity is stronger than in the Volland-Stern electric field simulation, with many transient spikes in the magnitude. The peak value is 6.1 MA during the first main phase, with spikes of 2–4 MA throughout 22 October (in particular, during the sawtooth oscillation injections early on that day), with a lingering intensity throughout the recovery phase of several tenths of a mega-amp. The eastward symmetric ring current increases from a prestorm value of <0.1 MA to a peak of 0.4 MA in the early recovery phase, tapering off slowly during 22 October. The second main phase of the storm interval does

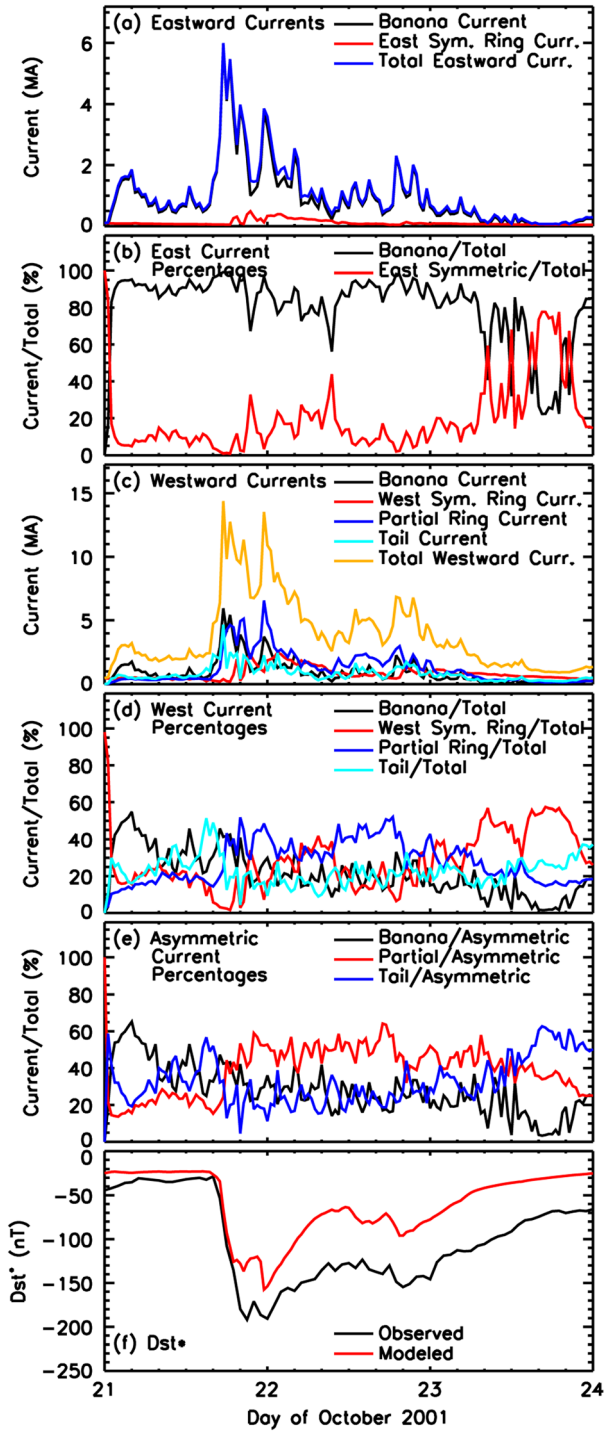

Figure 7. Analysis of currents from a HEIDI simulation with a S-C electric field of the 21 October 2001 magnetic storm. The panels are the same as in Figure 6.

not yield a significant eastward symmetric ring current, with a peak value from the second *Dst** intensification of only <0.2 MA late on 22 October.

[32] The dominance of the banana current over the eastward symmetric ring current is clearly seen in Figure 7b, which shows the percentages of these currents against their total. Only rarely does the eastward symmetric ring current carry a majority of the eastward current in the simulation domain, and these are often times when the banana current drops down rather than the ring current intensifying. This redistribution of the current away from symmetry towards an asymmetric component is what was expected in the presence of nonlinear feedback. That is, as mentioned earlier in this subsection, the electric field from the closure of the partial ring current will break up larger pressure peaks into smaller ones, creating new pressure peaks that each has its own banana current flowing around them. These fields will inhibit the sunward convective flow pattern through the inner magnetosphere and suppress and delay the formation of a symmetric ring current.

[33] Figure 7c presents the magnitudes of the westward currents. The lines often intersect as they all have peaks in the 1–6 MA range throughout the storm. The tail current peaks first, followed by the banana current, then the partial ring current is the largest system, with the symmetric ring current peaking in the recovery phase. None of the current systems, however, show a clear dominance of the total magnitude.

[34] To better quantify these relative contributions, Figure 7d converts the magnitudes into percentages of the total westward current. The same trends are seen here as in Figure 6d, with the tail current dominating the initial intensification, followed by the partial ring current, which eventually gives way to the symmetric ring current in the late recovery phase. The difference between the plots is that the peak percentages are systematically smaller in the self-consistent electric field simulation than in the Volland-Stern field run. The change has two causes: the first is that the tail and banana currents are larger in the self-consistent run; the second is that the partial and symmetric ring currents do not have as deep of minima in this run. The self-consistent electric field redistributes the current between the four current systems, yielding smaller peak percentages for the dominant loop.

[35] Figure 7e shows percentages of the three asymmetric current systems with respect to their summed magnitude. The trends of which current dominates during each part of the storm sequence are the same as with the Volland-Stern run results, but again the peak values are lower in this second run set-up. The dominant current system rarely carries more than 60% of the total, and there are many instances when the three current systems are nearly equally balanced. The banana current is the largest westward asymmetric current system only for a brief prestorm interval when the simulation initial conditions are still reconfiguring.

[36] The conclusions about the banana current from our analysis of these storm-time numerical simulations are as follows: The banana current can dominate the eastward current during the main phase of storms, but it gives way to dominance by the eastward symmetric ring current during quiet times. However, it never dominates the westward current in the inner magnetosphere, remaining below 20% during times of smooth pressure peak distributions and perhaps rising to 30%–40% during the main phase intervals with a highly structured pressure distribution.

4. Magnetic Perturbation Analysis

[37] It is useful to assess the magnetic perturbation signature related to this current system, especially relative to the other currents in near-Earth space. An estimate of the banana

current's contribution to ground-based magnetometer perturbation measurements can be done with an analytical assessment of near-Earth currents. The banana current can be greatly simplified into an idealized loop in the equatorial plane, with eastward and westward circular arcs of angular extent φ at geocentric radial distances a and b, respectively, and radial segments connecting the ends. A schematic of this current system is shown in Figure 8. We can further assume that there is a westward partial ring current of similar angular extent also at geocentric radial distance b. Eastward and westward symmetric ring currents will be considered at a and b, as well, each with a full 2π angular extent. A final current to include in this analysis is the cross-tail current, to be represented by its most intense, innermost extent, placed here at radial distance c (somewhere beyond b) with an angular extent of $\pi/2$.

[38] The Biot-Savart relation for line currents states that the magnetic field **B** has this form:

$$B = \frac{\mu_0 I}{4\pi} \int \frac{d1 \times \hat{r}}{r^2} \tag{3}$$

where I is the current magnitude, μ_0 is the permeability of free space, dl is a differential path length along the current loop, and **r** (with magnitude r and unit vector $\hat{r}$) is the vector from the location of the current to the location where we want to know **B**. For the radial components, the cross product yields zero, while for the circular current segments, the cross product yields the magnitudes of the two vectors, with this form:

$$B = \frac{\mu_0 I \varphi}{4\pi r} \tag{4}$$

[39] The resulting B is negative for westward currents and positive for eastward currents. The perturbation from the field-aligned closure currents will exactly cancel each other.

[40] Given this very simplistic equatorial plane current formulation, the four current systems (banana current, partial ring current, symmetric ring current, and tail current) then have these magnetic perturbation contributions:

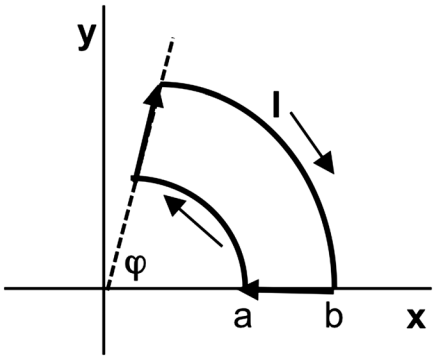

Figure 8. Idealized schematic of the banana current in the equatorial plane.

$$\begin{aligned}
\Delta B_{BC} &= \frac{\mu_0 I_{BC} \varphi}{4\pi} \left(\frac{1}{a} - \frac{1}{b} \right) \\
\Delta B_{BC} &= -\frac{\mu_0 I_{PRC} \varphi}{4\pi} \\
\Delta B_{SRC} &= \frac{\mu_0}{2} \left(\frac{I_{SRC-east}}{a} - \frac{I_{SRC-west}}{b} \right) \\
\Delta B_{TC} &= \frac{\mu_0 I_{TC}}{8c}
\end{aligned} \tag{5}$$

[41] Note that this formulation only includes the magnetospheric equatorial plane cross-field current contributions to the ground magnetic perturbation. Specifically, equation (5) omits the contributions from the non-equatorial plane closure of the partial ring current and the tail current. While these omissions need to be considered for a rigorous analysis, they are justified in this approximate formulation by considering, for the partial ring current, the cancellation of the closure current contribution in the idealized geometry of *Fukushima* [1969] and, for the tail current, the tail magnetopause is much farther away from the Earth than the near-Earth equatorial plane.

[42] It is interesting to note that the magnetic perturbation related to the banana current is positive because $a > b$. It will be rather small, however. From the idealized pressure pulse descriptions in Figure 1, it was found that I_{PRC} is 4–14 times larger than I_{BC}. Using the formulas in equation (5), the ratio of the magnetic perturbations from the banana current and partial ring currents is, therefore,

$$\frac{\Delta B_{BC}}{\Delta B_{PRC}} = \frac{b - a}{4a} \tag{6}$$

[43] If a and b are $L = 4$ and 6, respectively, then the perturbation ratio is 1:8, a similar number to the pressure analysis results in section 2. The conclusion is that an overwhelming majority of the ground-based measurement is from the partial ring current, not from the banana current.

[44] Let us briefly examine the magnetic perturbation related to the symmetric ring current. If we assume that the idealized pressure profiles in Figure 1 are applicable to the symmetric ring current (that is, this pressure peak is uniform in local time), then it means that the westward symmetric ring current is roughly 4–14 times larger than the eastward symmetric ring current. The radial distances of a and b, however, will not be different by a factor of 4 (it would rarely, if ever, exceed a factor of 2). Therefore, the symmetric ring current will typically produce a negative perturbation.

[45] A final comparison to be made is the size of the tail current perturbation relative to the main phase inner magnetospheric currents (specifically, the sum of the banana and partial ring currents). Let us assume that the tail current is equal to half of the partial ring current (so, $I_{\mathrm{PRC}} = 2I_{\mathrm{TC}} = 4\ I_{\mathrm{BC}}$), that c is located as far from b as is a (i.e., $c = b + (b - a) = 2\ b - a$), and that the angular extent of the banana and partial ring current is $\pi/3$, then we obtain

$$\frac{\Delta B_{PRC} + \Delta B_{BC}}{\Delta B_{TC}} = \frac{(5a - b)(2b - a)}{3ab} \tag{7}$$

[46] Plugging in our assumed values of $a = 4$ and $b = 6$, this ratio is 1.56, indicating that a majority of the ground-

based perturbation from asymmetric magnetospheric currents comes from the inner magnetospheric currents (i.e., the PRC and BC). If, however, I_{TC} is set equal to I_{PRC}, then the denominator of equation (7) becomes 6*ab*, and plugging in our assumed values, the ratio becomes 0.78. Therefore, depending on the relative magnitudes and spatial locations of the various localized current systems, they will each take a turn at dominating the asymmetric-current contributions to the magnetic perturbation at low latitudes on the ground.

[47] To put a number on the magnetic perturbation from the banana current, let us assume that $I_{BC} = 2$ MA, $\varphi = \pi/3$, $a = 4$ R_E and $b = 6$ R_E. These parameters yield a $\Delta\mathbf{B}_{BC}$ of +3 nT, which is a small contribution to the ground-based storm-time magnetic distortion, which peaked at −200 nT. Again, this is because of the competing contributions from the equal-magnitude east- and west-directed portions of the loop. It would be similarly negligible at radial distances beyond the banana current loop, for instance at geosynchronous orbit or in the near-Earth tail region. Again, the competing magnetic signatures from the two azimuthal portions of the loop would cancel most of the perturbation at such locations. This makes the banana current very difficult to detect from ground-based stations or geosynchronously orbiting satellites, implying that this current could, therefore, quite easily be ignored when the magnetosphere is viewed from either of these particular observational perspectives.

[48] There is hope for detecting a signature of the banana current, however. It flows clockwise around the pressure peak (when viewed from the north) and, therefore, the magnetic perturbation within the high-pressure region is southward from the entire banana current loop. The magnetic perturbation at the pressure peak from a 2 MA banana current is tens of nanotesla, which can be perhaps 10% of the total field strength for an inner magnetospheric location of 4 or 5 R_E. This is a non-negligible contribution to the field distortion in the inner magnetosphere and should be taken into account (although, it was not taken into account in the magnetic field for the simulation results presented above).

5. Discussion

[49] From the results presented above, it can be concluded that the banana current is a regular feature of the inner magnetosphere, with a magnitude reaching a few mega-amps during the main phases of storms. During extended quiet times, however, it can drop to amplitudes of less than 0.1 MA, essentially becoming negligible as a factor in distorting the inner magnetospheric magnetic field. Even though it flows westward along the outer portion of a plasma pressure peak, the banana current closes in a loop around the plasma pressure peak, making it distinct from the other current systems in near-Earth space. Specifically, it is not the same as the partial ring current, which we have defined as asymmetric currents that close along magnetic field lines and then through horizontal ionospheric Pedersen currents. It is not the same as the tail current, which we have defined as a current that closes along the magnetopause. It is not the same as the symmetric ring current, which we have defined as current that encircles the Earth within the inner magnetosphere. The banana current is its own current system and needs to be considered as such.

[50] Other studies have noted the presence of this current loop that is wholly contained within the magnetosphere yet does not circumscribe the Earth. Specifically, it has been seen in current patterns derived from energetic neutral atom (ENA) images of the inner magnetospheric plasma pressure [*Roelof et al*., 2004; *McKenna-Lawlor et al*., 2005]. These studies used inverted ENA observations across a broad range of particle energies to reconstruct the total plasma pressure distribution in near-Earth space. Then, using equation (1), currents were calculated and, by connecting the vectors, traced along current loops. In addition, numerical studies of current systems in the inner magnetosphere have also commented on the existence of this current system [e.g., *Liemohn et al*., 2011, 2012]. In particular, *Liemohn et al*. [2012] noted that it often exists at or near the equatorial plane (defined here as the minimum magnetic field surface), even while other current systems exist at higher latitudes along the same magnetic field line. The same conclusion can be drawn here, noting that it is usually the partial ring current that exists at higher latitudes on those field lines that also have banana current flowing perpendicular to it.

[51] To illustrate this, Figure 9 shows the simulation results from the Space Weather Modeling Framework (SWMF) [*Toth et al*., 2005, 2012] for an idealized simulation after a few hours of being driven by −5 nT southward interplanetary magnetic field. This simulation was conducted with the Block-Adaptive-Tree-Solarwind-Roe-Upwind-Scheme global magnetohydrodynamic (MHD) model, the Rice Convection Model, and the Ridley Ionosphere Model, two-way coupled by the SWMF and run to steady state. Shown is the plasma pressure in the x-y and x-z planes, radial current density on a 2.5 R_E sphere, and white line current traces, all from the MHD output. It shows that the banana current encircles the region of high pressure on the nightside inner magnetosphere, with partial ring current at higher latitudes along the same field lines and farther out on the pressure peak. Beyond this, a couple traces of the tail current are also included. This figure serves as a summarizing overview plot of the relationship of the various current systems in the near-Earth nightside magnetosphere. Note, however, that it does not include symmetric ring current. After a rigorous systematic search, a symmetric ring current trace was not found in these simulation results. This is informative, though, as it is a reminder that not every current system exists at all times in near-Earth space.

[52] The lack of a symmetric ring current in Figure 9 also highlights the possibility of the banana current and partial ring current eventually transforming into the symmetric ring current. Specifically, as a localized pressure peak azimuthally drifts in local time, it will also spread out in local time due to the energy-dependent azimuthal drift speeds. It will reach a state where the leading end will catch up with the trailing end, at which time, the radial components of the banana current will cancel and the loop will break into the eastward and westward symmetric ring currents. At this same time, the field-aligned currents closing the partial ring current will cancel, and the magnetospheric component of the partial ring current will become westward symmetric ring current. In short, all current systems do not have to exist simultaneously and should, in fact, naturally transform from one system to another.

[53] It should be pointed out that the banana current most likely exists near the equatorial plane, but it does not have to be strictly centered on it. The banana current can be shifted off the equator if the ionospheric conductances are unbalanced in the two conjugate footpoint regions. In a bounce-

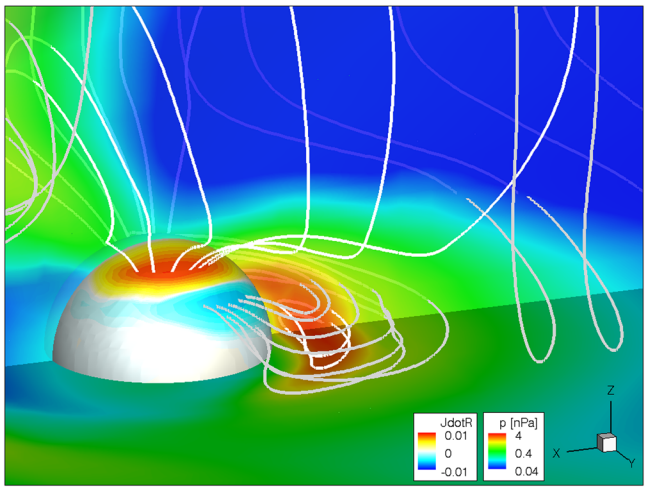

Figure 9. A 3-day rendering of an idealized SWMF simulation result. The color background on the two planar slices ($z = 0$ plane and $y = 0$ plane) is plasma pressure (red = large, blue = small) and on the $R = 2.5$ R_E sphere is radial current density (red = out of ionosphere, blue = into ionosphere). The white lines are current stream traces, showing a variety of current loop systems in the near-Earth nightside region, including tail current, partial ring current, and banana current.

averaged approximation, the particle distribution is symmetric about the equatorial plane; therefore, the spatial distribution of cross-field current is symmetric as well. It is reasonable to assume, then, that the field-aligned currents, whether into or out of the ionosphere, will split evenly around the equatorial plane and flow symmetrically into the conjugate footpoints. If the conductances are different at these two locations, though, the electric potentials will be different. Because it is a good conductor, the magnetic field line wants to be an equipotential and the north-south split for the field-aligned currents will therefore shift off the equator in the direction of lower conductance until the two hemispheric potential patterns match. While there is some communication and adjustment time for this to occur, the transit time of Alfven waves and electron transport along inner magnetospheric field lines is far smaller than the drift or loss timescales of the keV-energy ions dominating the plasma pressure.

[54] A caveat to remember about the conclusions of this study is that it is based on analytical estimations and two numerical simulations of a single magnetic storm interval. The absolute and relative magnitudes of the currents in section 3 are only those calculated by the physics contained in HEIDI and only within this model's spatial domain, which for these simulations extend out to geosynchronous orbit. The tail current, in particular, is certainly underestimated, and even the symmetric ring current, partial ring current, and banana current could be underestimated if any part of these systems exists outside of 6.6 R_E. Even though the *Dst** time series match fairly well for this storm, the method of converting the hot ion phase space densities into a magnetic perturbation is known to have limitations [e.g., *Carovillano and Siscoe*, 1973]. *Liemohn* [2003] found that there is a truncation current implicitly included in this method, which improves the *Dst** comparisons, but does not explain the current distribution beyond the simulation domain. Furthermore, the model used a dipole magnetic field, which overestimates the plasma drifts (and therefore plasma pressures) but underestimates the currents from a given plasma pressure. Even with these stipulations, the results presented above are useful in identifying and quantifying this unique current system within the inner magnetosphere.

[55] There are several possibilities for confirming the existence and properties of the banana current with existing observational assets. For one, the Two Wide-Angle Imaging Neutral-Atom Spectrometers on their highly elliptical, highly inclined Molniya orbits provide snapshots of the energetic neutral atom loss by-product from the keV ions of the inner magnetosphere. Inverting these images into pressure distributions and subsequently into current density distributions provides a global map of the local time asymmetries of the eastward and westward currents in near-Earth space. Additionally, the multiple satellites of the Time History of Events and Macroscale Interactions during Substorms and Van Allen Probes missions in near-equatorial orbit offer the chance to measure the magnetic perturbation in relation to the pressure peak. Using the methodology of section 2 above, a single radial pass through the inner magnetosphere could be used to calculate the ratio of the eastward to westward azimuthal currents. One satellite pass alone, however, cannot resolve the spatial structure of the pressure peak and therefore the closure path of these currents. Simultaneous radial passes from several satellites, however, could be compiled to form a data-based reconstruction of the pressure distribution, with the additional context of the local magnetic and electric fields. The methodology of section 4 could then be used to isolate the contributions from various current systems.

6. Summary

[56] It has been shown that the eastward current deep within the inner magnetosphere can be nonuniform in local time, indicating that it is not entirely a symmetric ring current, but rather is carried by some other current system. We assessed the closure paths of this extra eastward current and concluded that it had to close via a westward current

around the pressure peak. Because of this characteristic crescent shape, it was given the name banana current.

[57] Numerical experiments were examined to assess the occurrence frequency and magnitude of the banana current. It was found that it is essentially a permanent fixture of the inner magnetosphere, but its intensity can drop to insignificant (<0.1 MA) values during extended quiet times. During a storm main phase, though, it can reach values of several mega-amps, having a significant (although minor) contribution to the total current of the inner magnetosphere. The banana current is more intense and lasts longer in simulations with a self-consistent electric field rather than an analytically specified field description. It waxes and wanes in parallel with the partial ring current, usually maintaining a relationship of two to five times smaller magnitude than the system with the ionospheric closure path.

[58] It was found that this current system produces a small, almost negligible ground-based magnetometer signature. However, the magnetic perturbation within the high-pressure region can be a significant weakening of the field. These contrasting influences make it especially difficult to detect with magnetic field observations, unless a satellite passes through the plasma pressure peak.

[59] **Acknowledgments.** The authors would like to thank the US government for sponsoring this research, in particular research grants from NASA (NNX08AQ15G, NNX09AF45G, NNX10AQ34C, and NNX11AO60G) and NSF (ATM-0802705, ATM-0903596, and AGS-1102863). Support for NYG was provided by both Finnish and US sponsors, including the Academy of Finland. The authors also thank the International Space Science Institute (ISSI) in Bern, Switzerland for its support of an international team on "Resolving Current Systems in Geospace". Solar wind data (for *Dst** calculations and model inputs) were provided by CDAWeb at NASA GSFC in Greenbelt, Maryland, USA and *Dst* values were taken from WDC-2 in Kyoto, Japan. M. W. Liemohn would like to thank all of the students who have ever taken AOSS 450, Geophysical Electromagnetics, at the University of Michigan, for helping him to realize that some of the magnetostatic problems he was assigning had direct relevance to this project.

References

Alexeev I. I., E. S. Belenkaya, V. V. Kalegaev, Y. I. Feldstein, and A. Grafe (1996), Magnetic storms and magnetotail currents, *J. Geophys. Res.*, *101*, 7737.

Antonova, E. E. (2004), Magnetostatic equilibrium and current systems in the Earth's magnetosphere, Adv. *Space Res. 33*(5), 752–760.

Antonova, E. E., and N. Yu. Ganushkina (1997), Azimuthal hot plasma pressure gradients and dawn-dusk electric field formation, *J. Atmos. Solar-Terr. Phys.*, *59*(11), 1343–1354.

Antonova, E. E., and N. Yu. Ganushkina (2000), Inner magnetospheric currents and their role in the magnetosphere dynamics, *Phys. Chem. Earth (C)*, *25*(1–2), 23–26.

Birmingham, T. J. (1992), Birkeland currents in an anisotropic, magnetostatic plasma, *J. Geophys. Res.*, *97*, 3907.

Brandt, P. C., S. Ohtani, D. G. Mitchell, M.-C. Fok, E. C. Roelof, and R. Demajistre (2002a), Global ENA observations of the storm mainphase ring current: Implications for skewed electric fields in the inner magnetosphere, *Geophys. Res. Lett.*, *29*(20), 1954, doi:10.1029/2002GL015160.

Brandt, P. C., D. G. Mitchell, Y. Ebihara, B. R. Sandel, E. C. Roelof, J. L. Burch, and R. Demajistre (2002b), Global IMAGE/HENA observations of the ring current: Examples of rapid response to IMF and ring current-plasmasphere interaction, *J. Geophys. Res.*, *107*(A11), 1359, doi:10.1029/2001JA000084.

Buzulukova, N., M.-C. Fok, J. Goldstein, P. Valek, D. J. McComas, and P. C. Brandt (2010), Ring current dynamics in moderate and strong storms: Comparative analysis of TWINS and IMAGE/HENA data with the Comprehensive Ring Current Model, *J. Geophys. Res.*, *115*, A12234, doi:10.1029/2010JA015292.

Carovillano, R. L., and G. L. Siscoe (1973), Energy and momentum theorems in magnetospheric processes, *Rev. Geophys. Space Phys.*, *11*, 289.

Daglis, I. A. (2006), Ring current dynamics, *Space Sci. Rev.*, *124*(1-4), 183–202, doi:10.1007/s11214-006-9104-z.

Daglis, I. A., J. U. Kozyra, Y. Kamide, D. Vassiliadis, A. S. Sharma, M. W. Liemohn, W. D. Gonzalez, B. T. Tsurutani, and G. Lu (2003), Intense space storms: Critical issues and open disputes, *J. Geophys. Res.*, *108* (A5), 1208, doi:10.1029/2002JA009722.

Ganushkina, N. Yu., T. I. Pulkkinen, M. V. Kubyshkina, H. J. Singer, and C. T. Russell (2002), Modeling the ring current magnetic field during storms, *J. Geophys. Res.*, *107*, doi:10.1029/2001JA900101.

Ganushkina, N. Yu., T. I. Pulkkinen, M. V. Kubyshkina, H. J. Singer, and C. T. Russell (2004), Long-term evolution of magnetospheric current systems during storms, *Ann. Geophys.*, *22*, 1317–1334.

Ganushkina, N., M. Liemohn, M. Kubyshkina, R. Ilie, and H. Singer (2010), Distortions of the magnetic field by storm-time current systems in Earth's magnetosphere, *Ann. Geophys.*, *28*, 123–140.

Ganushkina, N. Y., S. Dubyagin, M. Kubyshkina, M. W. Liemohn, and A. Runov (2012), Inner magnetosphere currents during the CIR/HSS storm on July 21-23, 2009, *J. Geophys. Res.*, *117*, A00L04, doi:10.1029/2011JA017393.

Fok, M-C., J. U. Kozyra, A. F. Nagy, C. E. Rasmussen, and G. V. Khazanov (1993), A decay model of equatorial ring current and the associated aeronomical consequences, *J. Geophys. Res.*, *98*, 19,381.

Fok, M.-C., R. A. Wolf, R. W. Spiro, and T. E. Moore (2001), Comprehensive computational model of the earth's ring current, *J. Geophys. Res.*, *106*, 8417.

Fok, M.-C., et al. (2003), Global ENA image simulations, *Space Sci. Rev.*, *109*, 77.

Frank, L. A. (1970), Direct detection of asymmetric increases of extraterrestrial 'ring current' proton intensities in the outer radiation zone, *J. Geophys. Res.*, *75*, 1263.

Fukushima, N. (1969), Equivalence in ground geomagnetic effect of Chapman-Vestine's and Birkland-Alfvén's electric current systems for polar magnetic storms, *Rep. Ionos. Space Res. Jpn.*, *23*(3).

Henderson, M. G., G. D. Reeves, H. E. Spence, R. B. Sheldon, A.M. Jorgensen, J. B. Blake, and J. F. Fennell (1997), First energetic neutral atom images from Polar, *Geophys. Res. Lett.*, *24*, 67.

Ilie, R., M. W. Liemohn, M. F. Thomsen, J. E. Borovsky, and J. Zhang (2008), The influence of epoch time selection when doing superposed epoch analysis on ACE and MPA data, *J. Geophys. Res.*, *113*, A00A14, doi:10.1029/2008JA013241.

Iyemori, T. (1990), Storm-time magnetospheric currents inferred from mid-latitude geomagnetic field variations, *J. Geomagn. Geoelectr.*, *42*, 1249.

Jaggi, R. K., and R. A. Wolf (1973), Self-consistent calculation of the motion of a sheet of ions in the magnetosphere, *J. Geophys. Res.*, *78*, 2842.

Jordanova, V. K., J. U. Kozyra, G. V. Khazanov, A. F. Nagy, C. E. Rasmussen, and M.-C. Fok (1994), A bounce-averaged kinetic model of the ring current ion population, *Geophys. Res. Lett.*, *21*, 2785.

Jorgensen, A. M., H. E. Spence, W. J. Hughes, and H. J. Singer (2004), A statistical study of the global structure of the ring current, *J. Geophys. Res.*, *109*, A12204, doi:10.1029/2003JA010090.

Kalegaev, V. V., N. Yu. Ganushkina, T. I. Pulkkinen, M. V. Kubyshkina, H. J. Singer, and C. T. Russell (2005), Relation between the ring current and the tail current during magnetic storms, *Ann. Geophys.*, *23*, 523–533.

Katus, R., M. W. Liemohn, D. L. Gallagher, A. J. Ridley, and S. Zou (2012), Normalized superposed epoch analysis reveals two step main phase enhancement: Evidence for potential and inductive convection during intense geomagnetic events, *J. Geophys. Res.*, submitted, doi:10.1029/2012JA017915.

Kubyshkina, M., T. I. Pulkkinen, N. Yu. Ganushkina, and N. Partamies (2008), Magnetospheric currents during sawtooth events: Event-oriented magnetic field model analysis, *J. Geophys. Res.*, *113*, A08211, doi:10.1029/2007JA012983.

Liemohn, M. W. (2003), Yet another caveat to the Dessler-Parker-Sckopke relation, *J. Geophys. Res.*, *108*(A6), 1251, doi:10.1029/2003JA009839.

Liemohn, M. W., and P. C. Brandt (2005), Small-scale structure in the storm-time ring current, in *Inner Magnetosphere Interactions: New Perspectives from Imaging*, AGU Monogr. Ser, vol. *159*, edited by J. L. Burch, M. Schulz, and H. Spence, Am. Geophys. Un., Washington, DCp. *167*.

Liemohn, M. W., J. U. Kozyra, V. K. Jordanova, G. V. Khazanov, M. F. Thomsen, and T. E. Cayton (1999), Analysis of early phase ring current recovery mechanisms during geomagnetic storms, *Geophys. Res. Lett.*, *25*, 2845.

Liemohn, M. W., J. U. Kozyra, C. R. Clauer, and A. J. Ridley (2001), Computational analysis of the near-Earth magnetospheric current system, *J. Geophys. Res.*, *106*, 29,531.

Liemohn, M. W., A. J. Ridley, D. L. Gallagher, D. M. Ober, and J. U. Kozyra (2004), Dependence of plasmaspheric morphology on the electric field description during the recovery phase of the April 17, 2002 magnetic storm, *J. Geophys. Res.*, *109*(A3), A03209, doi:10.1029/2003JA010304.

Liemohn, M. W., A. J. Ridley, P. C. Brandt, D. L. Gallagher, J. U. Kozyra, D. G. Mitchell, E. C. Roelof, and R. DeMajistre (2005), Parametric analysis of nightside conductance effects on inner magnetospheric dynamics for the 17 April 2002 storm, *J. Geophys. Res.*, *110*, A12S22, doi:10.1029/2005JA011109.

Liemohn, M. W., A. J. Ridley, J. U. Kozyra, D. L. Gallagher, M. F. Thomsen, M. G. Henderson, M. H. Denton, P. C. Brandt, and J. Goldstein (2006), Analyzing electric field morphology through data-model comparisons of the GEM IM/S Assessment Challenge events, *J. Geophys. Res.*, *111*, A11S11, doi:10.1029/2006JA011700.

Liemohn, M. W., D. L. De Zeeuw, R. Ilie, and N. Yu. Ganushkina (2011), Deciphering magnetospheric cross-field currents, *Geophys. Res. Lett.*, *38*, L20106, doi:10.1029/2011GL049611.

Liemohn, M. W., D. L. De Zeeuw, N. Y. Ganushkina, J. U. Kozyra, and D. T. Welling (2012), Magnetospheric cross-field currents during the January 6-7, 2011, high-speed stream-driven interval, *J. Atmos. Solar-Terr. Phys.*, in press, doi:10.1016/j.jastp.2012.09.007.

Lui, A. T. Y. (2003), Inner magnetospheric plasma pressure distribution and its local time asymmetry, *Geophys. Res. Lett.*, *30*(16), 1846, doi:10.1029/2003GL017596.

Lui, A. T. Y. and D. C. Hamilton (1992), Radial profiles of quiet time magnetospheric parameters, *J. Geophys. Res.*, *97*(A12), 19,325–19,332, doi:10.1029/92JA01539.

Lui, A. T. Y., R. W. McEntire, and S. M. Krimigis (1987), Evolution of the ring current during two geomagnetic storms, *J. Geophys. Res.*, *92*, 7459.

Lui, A. T. Y., H. E. Spence, and D. P. Stern (1994), Empirical modeling of the quiet time nightside magnetosphere, *J. Geophys. Res.*, *99*(A1), 151–157, doi:10.1029/93JA02647.

Mauk, B. H., and L. J. Zanetti (1987), Magnetospheric electric fields and currents, *Rev. Geophys.*, *25*, 541.

Maynard, N. C., and A. J. Chen (1975), Isolated cold plasma regions: Observations and their relation to possible production mechanisms, *J. Geophys. Res.*, *80*, 1009.

McKenna-Lawlor, S., et al. (2005), An overview of the scientific objectives and technical configuration of the NeUtral Atom Detector Unit (NUADU) for the Chinese Double Star Mission, *Planet. Space Sci.*, *53*, 335–348, doi:10.1016/j.pss.2004.09.060.

Milillo, A., S. Orsini, and I. A. Daglis (2001), Empirical model of proton fluxes in the equatorial inner magnetosphere: Development, *J. Geophys. Res.*, *106*(A11), 25,713–25,729, doi:10.1029/2000JA900158.

Mitchell, D. G., K. C. Hsieh, C. C. Curtis, D. C. Hamilton, H. D. Voss, E. C. Roelof, and P. C. son-Brandt (2001), Imaging two geomagnetic storms in energetic neutral atoms, *Geophys. Res. Lett.*, *28*(6), 1151–1154, doi:10.1029/2000GL012395.

Ohtani, S., M. Nose, G. Rostoker, H. Singer, A. T. Y. Lui, and M. Nakamura (2001), Storm-substorm relationship: Contribution of the tail current to *Dst*, *J. Geophys. Res.*, *106*, 21,199.

Ohtani, S., Y. Ebihara, and H. J. Singer (2007), Storm-time magnetic configurations at geosynchronous orbit: Comparison between the main and recovery phases, *J. Geophys. Res.*, *112*, A05202, doi:10.1029/2006JA011959.

Parker, E. N. (2000), Newton, Maxwell, and magnetospheric physics, in *Magnetospheric Current Systems*, AGU Monogr. Ser, edited by S.-I. Ohtani, R. Fujii, M. Hesse, and R. L. Lysak, Am. Geophys. Un., Washington, D.C. vol. *118*, p. 1.

Perez, J. D., G. Kozlowski, P. C. son-Brandt, D. G. Mitchell, J.-M. Jahn, C. J. Pollock, and X. X. Zhang (2001), Initial ion equatorial pitch angle distributions from medium and high energy neutral atom images obtained by IMAGE, *Geophys. Res. Lett.*, *28*(6), 1155–1158, doi:10.1029/2000GL012636.

Pollock, C. J., et al. (2001), First medium energy neutral atom (MENA) Images of Earth's magnetosphere during substorm and storm-time, *Geophys. Res. Lett.*, *28*(6), 1147–1150, doi:10.1029/2000GL012641.

Pulkkinen, T. I., N. Y. Ganushkina, E. I. Tanskanen, M. Kubyshkina, G. D. Reeves, M. F. Thomsen, C. T. Russell, H. J. Singer, J. A. Slavin, and J. Gjerloev (2006), Magnetospheric current systems during stormtime sawtooth events, *J. Geophys. Res.*, *111*, A11S17, doi:10.1029/2006JA011627.

Pulkkinen, T. I., N. Partamies, K. E. J. Huttunen, G. D. Reeves, and H. E. J. Koskinen (2007), Differences in geomagnetic storms driven by magnetic clouds and ICME sheath regions, *Geophys. Res. Lett.*, *34*, L02105, doi:10.1029/2006GL027775.

Ridley, A. J., and M. W. Liemohn (2002), A model-derived description of the penetration electric field, *J. Geophys. Res.*, *107*(A8), 1151, doi:10.1029/2001JA000051.

Roelof, E. C. (1987), Energetic neutral atom image of a storm-time ring current, *Geophys. Res. Lett.*, *14*(6), 652–655, doi:10.1029/GL014i006p00652.

Roelof, E. C., P. C. Brandt, and D. G. Mitchell (2004), Derivation of currents and diamagnetic effects from global plasma pressure distributions obtained by IMAGE/HENA, *Adv. Space Res.*, *33*, 747–751.

Runov, A., V. Angelopoulos, N. Ganushkina, R. Nakamura, J. McFadden, D. Larson, I. Dandouras, K.-H. Glassmeier, and C. Carr (2008), Multipoint observations of the inner boundary of the plasma sheet during geomagnetic disturbances, *Geophys. Res. Lett.*, *35*, L17S23, doi:10.1029/2008GL033982.

Siscoe, G. L., N. U. Crooker, G. M. Erickson, G. U. O. Sonnerup, K. D. Siebert, D. R. Weimer, W. W. White, and N. C. Maynard (2000), Global geometry of magnetospheric currents inferred from MHD simulations, in *Magnetospheric Current Systems*, AGU Monogr. Ser, ed. by S.-I. Ohtani, R. Fujii, M. Hesse, and R. L. Lysak, Am. Geophys. Un., Washington, D. C, vol. *118*, p. 41.

Stern, D. P. (1975), The motion of a proton in the equatorial magnetosphere, *J. Geophys. Res.*, *80*, 595.

Toth, G., et al. (2005), Space Weather Modeling Framework: A new tool for the space science community, *J. Geophys. Res.*, *110*, A12226, doi:10.1029/2005JA011126.

Toth, G. et al. (2012), Adaptive numerical algorithms in space weather modeling, *J. Comput. Phys.*, *231*, 870.

Tsyganenko, N. A., H. J. Singer, and J. C. Kasper (2003), Storm-time distortion of the inner magnetosphere: How severe can it get?, *J. Geophys. Res.*, *108*(A5), 1209, doi:10.1029/2002JA009808.

Turner, N. E., D. N. Baker, T. I. Pulkkinen, and R. L. McPherron (2000), Evaluation of the tail current contribution to *Dst*, *J. Geophys. Res.*, *105*, 5431.

Valek, P., P. C. Brandt, N. Buzulukova, M.-C. Fok, J. Goldstein, D. J. McComas, J. D. Perez, E. Roelof, and R. Skoug (2010), Evolution of low-altitude and ring current ENA emissions from a moderate magnetospheric storm: Continuous and simultaneous TWINS observations, *J. Geophys. Res.*, *115*, A11209, doi:10.1029/2010JA015429.

Vasyliunas, V. M. (1970), Mathematical models of magnetospheric convection and its coupling to the ionosphere, in Particles and Fields in the Magnetosphere, edited by B. M. McCormac, D. Riedel, Hingham, MA, p. 60.

Volland, H. (1973), A semiempirical model of large-scale magnetospheric electric fields, *J. Geophys. Res.*, *78*, 171.